Proceeding Paper

The Low-Energy Module (LEM): Development of a CubeSat Spectrometer for Sub-MeV Particles and Gamma-Ray Burst Detection †

Riccardo Nicolaidis [1,2,*,‡], Francesco Nozzoli [1,2,‡], Giancarlo Pepponi [3,‡], Pierluigi Bellutti [3,‡], Evgeny Demenev [3,‡], Francesco Maria Follega [1,2,‡], Roberto Iuppa [1,2,‡] and Veronica Vilona [1,2,‡]

1 Department of Physics, University of Trento, 38123 Trento, Italy
2 INFN—Trento Institute of Fundamental Physics and Applications, 38123 Trento, Italy
3 Fondazione Bruno Kessler, 38123 Trento, Italy
* Correspondence: riccardo.nicolaidis@unitn.it
† Presented at the 2nd Electronic Conference on Universe, 16 February–2 March 2023; Available online: https://ecu2023.sciforum.net/.
‡ These authors contributed equally to this work.

Abstract: An accurate flux measurement of low-energy charged particles trapped in the magnetosphere is necessary for space weather characterization and to study the coupling between the lithosphere and magnetosphere, which allows for the investigation of the correlations between seismic events and particle precipitation from Van Allen belts. In this work, the project of a CubeSat space spectrometer, the Low-Energy Module (LEM), is shown. The detector will be able to perform an event-based measurement of the energy, arrival direction, and composition of low-energy charged particles down to 0.1 MeV. Moreover, thanks to a CdZnTe mini-calorimeter, the LEM spectrometer also allows for photon detection in the sub-MeV range, joining the quest for the investigation of the nature of Gamma-ray bursts. The particle identification of the LEM relies on the $\Delta E - E$ technique performed by thin silicon detectors. This multipurpose spectrometer will fit within a $10 \times 10 \times 10$ cm^3 CubeSat frame, and it will be constructed as a joint project between the University of Trento, FBK, and INFN-TIFPA. To fulfil the size and mass requirements, an innovative approach, based on active particle collimation, was designed for the LEM; this avoids the heavy/bulky passive collimators of previous space detectors. In this paper, we will present the LEM geometry, its detection concept, and the results from the developed GEANT4 simulation.

Keywords: low-energy module; low-energy particles; gamma-ray bursts; space weather; cubesat; $\Delta E - E$ technique

1. Introduction

The Low-Energy Module (LEM) will be a compact spectrometer able to perform an event-based measurement of the energy, direction, and composition of low-energy charged particles, in particular, down to 0.1 MeV for electrons. The physics goal of this detector is the monitoring of the magnetosphere and ionosphere environment. It is known that the measurements of the fluxes of low energetic particles may allow the characterisation of the coupling between the lithosphere, atmosphere, ionosphere, and magnetosphere. In particular, earthquakes are dynamic processes caused by continuous and slow strain accumulation. From studies on fault rupture mechanics, seismic wave propagation, and geophysical parameters measured in the ionosphere and the low magnetosphere, some anomalies correlated with catastrophic events were discovered. Moreover, statistical evidence of a temporal correlation between particle precipitations from Van Allen belts and strong seismic events has been pointed out [1]. These observations motivate interest in further detailed measurements of electron fluxes in the energy window 0.1–7 MeV, which may be a promising channel for identifying possible seismic precursors.

Another interesting case study for the LEM instrument is its application to space weather. Severe space weather storms can cause power outages and telecommunication alterations. For this reason, the construction of new instruments to monitor and (possibly) predict the effects of solar activity on Earth is crucial.

The LEM will be a particle telescope performing an event-based measurement of the energy, direction, and composition of low-energy charged particles, in particular, electrons down to 0.1 MeV. This capability is not possible with the existing detectors, for which the possibility of an event-based PID or the possibility of monitoring the particle flux from different directions at the same time fails or are not able to measure the directions of low-energy particles because of the multiple scattering occurring in the first layer of a particle-tracking configuration.

2. The Current Landscape of Space-Based Particle Detectors

Extensive literature exists about particle detectors in space using silicon technologies. The instruments under examination, are as follows: the Instrument for the Detection of Particles (IDP) on the DEMETER microsatellite [2–4], the High-Energy Particle Package (HEPP-H and HEPP-L) on CSES [5–8], the Mars Energetic Particle Analyzer (Mars-EPA) on the Tianwen-1 mission [9–11], and the Radiation Assessment Detector on the Curiosity rover [12–16].

Some of the most important features of these instruments are listed in Table 1. Even though all of these experiments have different scientific purposes and goals, their detection concepts and schemes are very similar, allowing a comparison between their structure, size, components, and performances. In Table 1, the reader can see a summary of the features characterising the previously mentioned experiments. By comparing the six detectors studied, we can conclude that the larger the number of layers inserted into the design, the better the performances in detecting energetic particles. Furthermore, by adding additional layers at the bottom of the instrument, as we can see in the RAD, on the Curiosity mission, or in the Mars-EPA that the maximum energy can be detected with an increase in the particle identification. On the other hand, to minimise the low-energy threshold, one has to minimise the thickness of the ΔE layer. As an example, the Mars-EPA, can detect electrons in the energy range of 0.1–2 MeV by adopting a ΔE layer made of passivated implanted planar silicon (PIPS) detectors with a thickness of 15 μm. Finally, the use of an inorganic scintillator as a calorimeter could be problematic. In particular, many scintillator crystals, such as Sodium-Iodide or Caesium-Iodide, are very fragile and hygroscopic. These aspects will unavoidably result in the introduction of mechanical supports or metallic wrapping, providing additional dead layers in which particles could deposit part of their energy.

Table 1. Summary of some features of the detectors studied in this section. The references from which I extracted the information are quoted within the text.

Instrument	Size Weight	Directions	Angular Resolution	Energy Range	PID	Detector Elements
IDP DEMETER	525 g	1	FOV 32 deg.	e: [0.07, 0.8] MeV	No	Silicon Diode
RAD Curiosity	∼10 × 10 × 10 cm^3	Complex segmentation	FOV 36.7 deg.	e: [0.1, 20] MeV p: [5, 200] MeV α: [5, 200] MeV l.Z: [10, 300] MeV	Yes	PIPS (3 segments) CsI(Tl) Plast. Scint.
HEPP-L	Large Collimators	5 Narrow 4 Wide	FOV 6.5 deg. FOV 15 deg.	e: [0.1, 3] MeV p: [2, 20] MeV	Yes	Si det. (2 layers) Plast. Scint.

Table 1. *Cont.*

Instrument	Size Weight	Directions	Angular Resolution	Energy Range	PID	Detector Elements
Mars-EPA	$270 \times 180 \times 148$ cm^3	1	FOV 60 deg.	e: [0.1, 12] MeV p: [2, 100] MeV α: [25, 400] MeV l.Z: [25, 400] MeV	Yes	PIPS (2 layers) CsI(Tl)

Furthermore, it is required that the LEM is compact (within $10 \times 10 \times 10$ cm^3) and that it can monitor the particle flux in a large field of view from different directions at the same time. These capabilities are not simultaneously fulfilled by the past detectors. Therefore, a different and innovative design is required for the LEM.

3. The LEM Concept: The Active Collimation Technique

The idea that allows for a reduction in the weight and size of the LEM detector relies on the active collimation technique. More precisely, a drilled plastic scintillator is acting as a veto. Only particles with the directions aligned with 1 of the 16 channels are detected by 1 of the 16 silicon sensor pairs. Thus, the direction information is obtained. Particles with the wrong direction are stopped in the aluminium shield or will release a signal in the drilled plastic scintillator veto. This technique is an alternative to the tracking one affected by the multiple scattering problem. On the other hand, the low density of the plastic scintillator veto avoids the significant weight required by a totally passive metallic collimator. However, the price to pay is a relatively high veto rate. This high veto rate will unavoidably result in an enhancement of the dead time of the detector. For this reason, a small drilled aluminium shield is still necessary to suppress very low-energy particles.

In Figure 1, the detection concept and a schematised cross-section of the instrument are shown. From the top, we can see the drilled aluminium mask suppressing the flux of very low energetic particles. Below the aluminium shield, the active anti-coincidence is obtained by using a drilled plastic scintillator (polyvinyl toluene). The aluminium drilled mask and the drilled anti-coincidence detector (ACD) define the so-called active collimator.
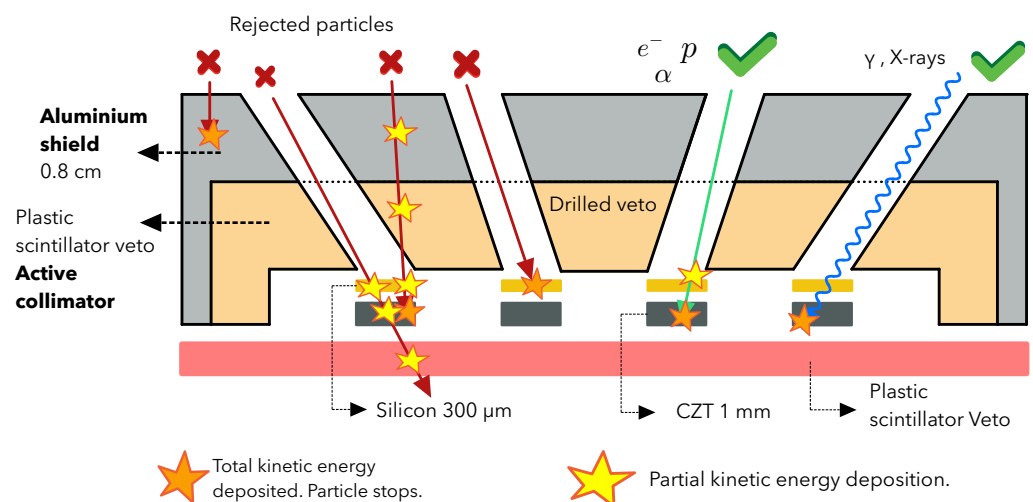

Figure 1. Detection concept embedded within the detector's geometry. The legend allows for distinguishing a partial energy deposition from a total kinetic energy deposition. In the picture, red trajectories represent discarded events, green trajectories represent good/accepted particle events, the blue trajectory represents a good/accepted photon event.

For an LEM operating in Low Earth Orbit (LEO), an aluminium thickness larger than 0.5 cm is necessary to reduce the veto rate from several MHz to the affordable rate

of $\sim$ kHz. Below the active collimation system, we place the 16 independent $\Delta E - E$ modules. These $\Delta E - E$ modules will measure the angular flux of particles crossing the veto channels ($\oslash$1 cm $\times$ 1.3 cm), encoding one specific solid angle in the sky with a resolution of 6°–7°. The sizes of the commercially available PIPS detectors manufactured by Ametek (50 mm^2–$\oslash$ 8 mm each) have been considered to define a realistic geometry in the detector simulation. The ΔE detector consists of a 100 µm thick PIPS detector while the E detector is a CdZnTe (or CZT) detector with a 1 mm thickness. These two $\Delta E - E$ layers allow a good particle identification in the energy ranges of approximately 0.1–10 MeV for electrons, 3–30 MeV for protons, and 10–100 MeV for alpha particles. A bottom plastic scintillator (ACD) is added at the very end of the LEM to ensure that the energy release is confined within the above layers. In particular, particle identification (PID) is not possible for the energetic particles crossing the ACD nor for slow particles stopped in the front PIPS. Events with an undefined direction are rejected thanks to a signal released in the active veto/collimator. Finally, events that are fully contained within the LEM, are selected. In this very last case, the direction is well defined, and it is also possible to perform an accurate PID. Thanks to the high density and high averaged atomic number of CZT [17,18], the LEM can identify low-energy γ-rays converting in the CdZnTe (CZT) mini-calorimeter and using all the surrounding low-Z sensors as anticoincidence. The ability to observe energetic photons will allow for the additional use of this compact particle spectrometer as a Gamma-ray burst (GRB) monitor [19].

4. Performance Characterisation with GEANT 4 Simulation

The detection concept adopted in the LEM is a consolidated technique denominated $\Delta E - E$ [20–22]. Basically, a $\Delta E - E$ particle spectrometer is composed of a thin detection layer and a thicker one behind. When a particle impinges on the spectrometer, if the kinetic energy is enough, the particle can cross the first layer, releasing a part of its kinetic energy ΔE. Then, the residual kinetic energy E can be deposited entirely within a second, thicker layer. This experimental layout allows for particle identification by measuring the energy deposited in the thinner layer, the ΔE energy, as well as the energy deposited in the thick sensor, the E energy. If a sub-MIP particle passes through a thin detector layer, the energy deposited, ΔE, will be velocity dependent:

$$\Delta E \approx \frac{Z^2}{\beta^2} \tag{1}$$

where Z is the projectile's charge, and β is its velocity in natural units. On the other hand, the residual kinetic energy, E, of a particle stopping in a subsequent thick detector is also velocity dependent:

$$E = mc^2(\gamma - 1) \approx \frac{1}{2}m(\beta c)^2 \tag{2}$$

where the non-relativistic approximation holds for sub-MIP particles. Therefore, in a $\Delta E - E$ spectrometer, a useful PID classifier can be defined in the following way:

$$\text{PID}_{\text{classifier}} = \log_{10}\left[\frac{\Delta E}{1\,\text{MeV}}\frac{E}{1\,\text{MeV}}\right] \approx \text{constant} + \log_{10} Z^2\left(\frac{mc^2}{1\,\text{MeV}}\right) \tag{3}$$

This PID$_{\text{classifier}}$ allows for the removal of the main dependence on the particle's velocity for sub-MIP particles; therefore, it is mainly dependent only on the particle's nature. For the LEM detector, this approximation is very good for protons and other nuclei, but, for electrons in the LEM kinetic energy range, the sub-MIP approximation fails, and the PID classifier for electrons will grow roughly according to $\log_{10}\frac{E}{1\,\text{MeV}}$. However, a good identification of the electrons from the protons, based on this classifier, is still achieved thanks to the fact that the proton mass is 2000 times larger than the electron mass. In Figure 2, the results from a GEANT4 [23] simulation are shown. In particular, the PID vs. the energy identification capability for the case of a mini-calorimeter made of 500 µm of

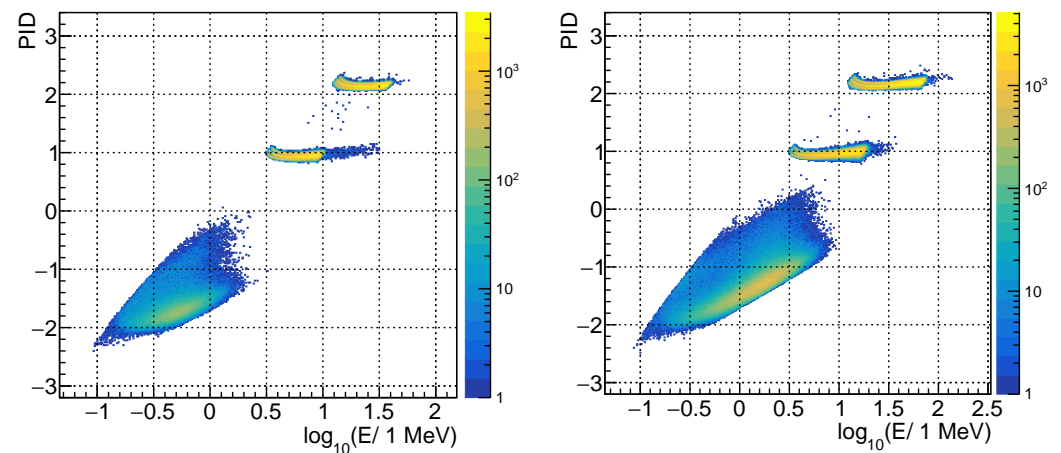silicon (left plot) is compared with the case of a mini-calorimeter composed of a 1 mm thick CZT.

Figure 2. PID classifier vs. kinetic energy. **Left**: 100 μm–500 μm PIPS detectors. **Right**: 100 μm PIPS and 1 mm CZT detectors. The three different clusters in each plot represent (from the top to the bottom): alpha particles, protons, electrons.

Finally, to quantify the advantage of the use of CZT sensors in the LEM as a monitor for GRBs, a comparison of the relative photon detection efficiency for the two mini-calorimeter configurations is shown in Figure 3.
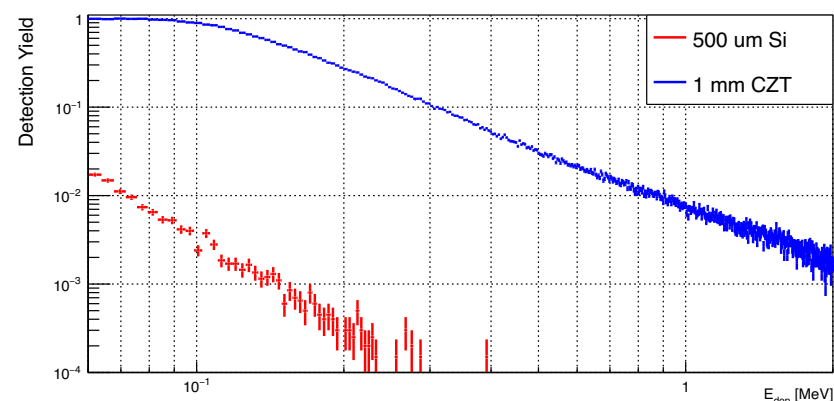

Figure 3. Improvement of detection yield for γ-rays thanks to CZT sensors. The legend refers to the material and the thickness considered for the E detector.

5. Conclusions and Outlooks

In this work, we described the Low-Energy Module (LEM): a compact particle spectrometer, suitable for a CubeSat, for measurement of the differential flux of low-energy particles in the lower magnetosphere. Here, it is worth summarising the structure of the LEM. To avoid a bulky and heavy detector, we designed an active collimator based on a thin aluminium shield followed by an anti-coincidence detector. The drilled aluminium shield protects the drilled ACD, made of a plastic scintillator, from the large flux of very low energetic electrons in LEO. The holes in the aluminium and in the ACD are used to select a known direction of the particles with an angular resolution of $6°$–$7°$. The LEM field of view is $60° \times 60°$, monitoring 16 directions in the sky at the same time. The particle identification relies on a series of 16 $\Delta E - E$ modules, based on the PIPS and CdZnTe detectors, placed below each collimator channel. An additional layer of plastic scintillator at the bottom is added as a veto to identify non-contained particles. Tests on sensor prototypes are ongoing at the INFN-TIFPA laboratory.

Abbreviations

The following abbreviations are used in this manuscript:

ACD	Anti-Coincidence Detector
CZT	Cadmium Zing Telluride (CdZnTe)
GEANT	Geometrty And Tracking
GRB	Gamma-Ray Burst
LAIM	Lithosphere Atmosphere Ionosphere Magnetosphere
LEM	Low-Energy Module
LEO	Low Earth Orbit
MILC	Magnetosphere Ionosphere Lithosphere Coupling
MIP	Minimum Ionising Particle
PID	Particle Identification
PIPS	Passivated Implanted Planar Silicon

References

1. Battiston, R.; Vitale, V. First evidence for correlations between electron fluxes measured by NOAA-POES satellites and large seismic events. *Nucl. Phys.-Proc. Suppl.* **2013**, *243*, 249–257. [CrossRef]
2. Parrot, M.; Li, M. Demeter results related to seismic activity. *Ursi Radio Sci. Bull.* **2015**, *2015*, 18–25.
3. Sauvaud, J.; Moreau, T.; Maggiolo, R.; Treilhou, J.P.; Jacquey, C.; Cros, A.; Coutelier, J.; Rouzaud, J.; Penou, E.; Gangloff, M. High-energy electron detection onboard DEMETER: The IDP spectrometer, description and first results on the inner belt. *Planet. Space Sci.* **2006**, *54*, 502–511. [CrossRef]
4. Dubourg, V.; Kainov, V.; Thoby, M.; Silkin, O.; Solovey, V. The DEMETER micro satellite launch campaign: A cheap access to space. *Adv. Space Res.* **2006**, *37*, 754–760. [CrossRef]
5. Xu, Y.B.; Wang, H.Y.; Meng, X.C.; Wang, H.; Lu, H.; Ma, Y.Q.; Li, X.Q.; Shi, F.; Wang, P.; Zhao, X.Y.; et al. Design and simulations for the detector based on DSSSD. *Chin. Phys. C* **2010**, *34*, 1846. [CrossRef]
6. Wu, F.; Wang, H.Y.; Zhao, X.Y.; Meng, X.C.; Xu, Y.B.; Wang, H.; Ma, Y.Q.; Lu, H.; Wang, P.; Shi, F.; et al. Design and performance study of the LEPD silicon tracker onboard the CSES satellite. *Chin. Phys. C* **2013**, *37*, 026004. [CrossRef]
7. Li, X.; Xu, Y.; An, Z.; Liang, X.; Wang, P.; Zhao, X.; Wang, H.; Lu, H.; Ma, Y.; Shen, X.; et al. The high-energy particle package onboard CSES. *Radiat. Detect. Technol. Methods* **2019**, *3*, 1–11. [CrossRef]
8. Nan, Y.F.; An, Z.H.; Li, H.X.; Zhao, X.Y.; Wen, X.Y.; Zhang, D.L.; Cheng, S.G.; Li, X.Q.; Wang, H.; Liang, X.H.; et al. Design and performance study of the HEPP-H calorimeter onboard the CSES satellite. *Res. Astron. Astrophys.* **2018**, *18*, 154. [CrossRef]
9. Li, C.; Tang, S.; Hu, X.; Qian, Y.; Wang, Y.; Zhao, H.; Fu, Q.; Sun, Z.; He, H.; Yu, Y.; et al. Design and realization of China Tianwen-1 energetic particle analyzer. *Space Sci. Rev.* **2021**, *217*, 1–20. [CrossRef]
10. Tang, S.; Wang, Y.; Zhao, H.; Fang, F.; Qian, Y.; Zhang, Y.; Yang, H.; Li, C.; Fu, Q.; Kong, J.; et al. Calibration of Mars energetic particle analyzer (MEPA). *Earth Planet. Phys.* **2020**, *4*, 355–363. [CrossRef]
11. Zou, Y.; Zhu, Y.; Bai, Y.; Wang, L.; Jia, Y.; Shen, W.; Fan, Y.; Liu, Y.; Wang, C.; Zhang, A.; et al. Scientific objectives and payloads of Tianwen-1, China's first Mars exploration mission. *Adv. Space Res.* **2021**, *67*, 812–823. [CrossRef]
12. Hassler, D.M.; Zeitlin, C.; Wimmer-Schweingruber, R.; Böttcher, S.; Martin, C.; Andrews, J.; Böhm, E.; Brinza, D.; Bullock, M.; Burmeister, S.; et al. The radiation assessment detector (RAD) investigation. *Space Sci. Rev.* **2012**, *170*, 503–558. [CrossRef]

13. Zeitlin, C.; Hassler, D.; Wimmer-Schweingruber, R.; Ehresmann, B.; Appel, J.; Berger, T.; Böhm, E.; Böttcher, S.; Brinza, D.; Burmeister, S.; et al. Calibration and characterization of the radiation assessment detector (RAD) on curiosity. *Space Sci. Rev.* **2016**, *201*, 201–233. [CrossRef]

14. Ehresmann, B.; Zeitlin, C.; Hassler, D.M.; Wimmer-Schweingruber, R.F.; Böhm, E.; Böttcher, S.; Brinza, D.E.; Burmeister, S.; Guo, J.; Köhler, J.; et al. Charged particle spectra obtained with the Mars Science Laboratory Radiation Assessment Detector (MSL/RAD) on the surface of Mars. *J. Geophys. Res. Planets* **2014**, *119*, 468–479. [CrossRef]

15. Ehresmann, B.; Hassler, D.M.; Zeitlin, C.; Guo, J.; Köhler, J.; Wimmer-Schweingruber, R.F.; Appel, J.K.; Brinza, D.E.; Rafkin, S.C.; Böttcher, S.I.; et al. Charged particle spectra measured during the transit to Mars with the Mars Science Laboratory Radiation Assessment Detector (MSL/RAD). *Life Sci. Space Res.* **2016**, *10*, 29–37. [CrossRef] [PubMed]

16. Guo, J.; Zeitlin, C.; Wimmer-Schweingruber, R.F.; Hassler, D.M.; Ehresmann, B.; Köhler, J.; Böhm, E.; Böttcher, S.; Brinza, D.; Burmeister, S.; et al. MSL-RAD radiation environment measurements. *Radiat. Prot. Dosim.* **2015**, *166*, 290–294. [CrossRef]

17. Takahashi, T.; Watanabe, S. Recent progress in CdTe and CdZnTe detectors. *IEEE Trans. Nucl. Sci.* **2001**, *48*, 950–959. [CrossRef]

18. Sordo, S.D.; Abbene, L.; Caroli, E.; Mancini, A.M.; Zappettini, A.; Ubertini, P. Progress in the development of CdTe and CdZnTe semiconductor radiation detectors for astrophysical and medical applications. *Sensors* **2009**, *9*, 3491–3526. [CrossRef]

19. Piran, T. The physics of gamma-ray bursts. *Rev. Mod. Phys.* **2005**, *76*, 1143. [CrossRef]

20. Scarduelli, V.; Gasques, L.; Chamon, L.; Lépine-Szily, A. A method to optimize mass discrimination of particles identified in $\Delta E - E$ silicon surface barrier detector systems. *Eur. Phys. J. A* **2020**, *56*, 1–7. [CrossRef]

21. Evensen, L.; Westgaard, T.; Avdeichikov, V.; Carlen, L.; Jakobsson, B.; Murin, Y.; Martensson, J.; Oskarsson, A.; Siwek, A.; Whitlow, H.; et al. Thin detectors for the CHICSi/spl Delta/EE telescope. *IEEE Trans. Nucl. Sci.* **1997**, *44*, 629–634. [CrossRef]

22. Carboni, S.; Barlini, S.; Bardelli, L.; Le Neindre, N.; Bini, M.; Borderie, B.; Bougault, R.; Casini, G.; Edelbruck, P.; Olmi, A.; et al. Particle identification using the $\Delta E - E$ technique and pulse shape discrimination with the silicon detectors of the FAZIA project. *Nucl. Instrum. Methods Phys. Res. Sect. A Accel. Spectrometers Detect. Assoc. Equip.* **2012**, *664*, 251–263. [CrossRef]

23. Agostinelli, S.; Allison, J.; Amako, K.; Apostolakis, J.; Araujo, H.; Arce, P.; Asai, M.; Axen, D.; Banerjee, S.; Barrand, G.; et al. GEANT4—A simulation toolkit. *Nucl. Instrum. Methods Phys. Res. Sect. A Accel. Spectrometers Detect. Assoc. Equip.* **2003**, *506*, 250–303. [CrossRef]